Gakh *et al.*
Acta Neuropathologica Communications (2024) 12:146
https://doi.org/10.1186/s40478-024-01854-4

Acta Neuropathologica Communications

RESEARCH

Open Access

Infrared spectral profiling of demyelinating activity in multiple sclerosis brain tissue

Oleksandr Gakh[1†], Jordan M. Wilkins[1†], Yong Guo[1], Bogdan F. Popescu[2,3], Stephen D. Weigand[4], Alicja Kalinowska-Lyszczarz[5] and Claudia F. Lucchinetti[6*]

Abstract

Multiple sclerosis (MS) is a leading cause of non-traumatic disability in young adults. The highly dynamic nature of MS lesions has made them difficult to study using traditional histopathology due to the specificity of current stains. This requires numerous stains to track and study demyelinating activity in MS. Thus, we utilized Fourier transform infrared (FTIR) spectroscopy to generate holistic biomolecular profiles of demyelinating activities in MS brain tissue. Multivariate analysis can differentiate MS tissue from controls. Analysis of the absorbance spectra shows profound reductions of lipids, proteins, and phosphate in white matter lesions. Changes in unsaturated lipids and lipid chain length indicate oxidative damage in MS brain tissue. Altered lipid and protein structures suggest changes in MS membrane structure and organization. Unique carbohydrate signatures are seen in MS tissue compared to controls, indicating altered metabolic activities. Cortical lesions had increased olefinic lipid content and abnormal membrane structure in normal appearing MS cortex compared to controls. Our results suggest that FTIR spectroscopy can further our understanding of lesion evolution and disease mechanisms in MS paving the way towards improved diagnosis, prognosis, and development of novel therapeutics.

Keywords Biomolecular profiling, Cortex, Demyelinating activity, Human brain tissue, Fourier transform infrared spectroscopy, Lesions, Multiple sclerosis, Sparse partial least squares-discriminant analysis, White matter

Introduction

Lesion development in multiple sclerosis (MS) is a dynamic and heterogenous process presenting differently across patients [18]. This complicates traditional immunohistochemical studies of human MS brain tissue as target-specific stains fail to encompass complex disease-related changes, especially biochemical alterations, that occur. This has made it challenging to understand the pathogenesis of MS and has impaired our ability to develop effective therapeutics that can halt and reverse progression in MS resulting in one of the leading causes of non-traumatic disability in young adults. Therefore, there is a dire need to establish new approaches that can provide a more comprehensive analysis of changes occurring at the different stages of demyelinating activity in MS lesions and greater insight into disease mechanisms.

†Oleksandr Gakh and Jordan M. Wilkins have contributed equally to this work.

*Correspondence:
Claudia F. Lucchinetti
claudia.lucchinetti@austin.utexas.edu
[1] Department of Neurology, Mayo Clinic, Rochester, MN 55905, USA
[2] Department of Anatomy, Physiology, and Pharmacology, University of Saskatchewan, Saskatoon, SK S7K 0M7, Canada
[3] Cameco MS Neuroscience Research Center, University of Saskatchewan, Saskatoon, SK S7K 0M7, Canada
[4] Department of Health Sciences Research, Mayo Clinic, Rochester, MN 55905, USA
[5] Department of Neurology, Division of Neurochemistry and Neuropathology, Poznan University of Medical Sciences, 49 Przybyszewskiego Street, 60-355 Poznan, Poland
[6] Department of Neurology, Frank and Charmaine Denius Dean's Chair in Medical Leadership, Dean of Dell Medical School, Senior Vice President Medical Affairs, University of Texas at Austin, Austin, TX 78712, USA

Several stages of demyelinating activity have been described in MS. In the early phase of MS, active white matter lesions are characterized by inflammation and an infiltration of microglia and macrophages, which can produce reactive oxygen species resulting in oxidative damage to lipids, proteins, nucleic acids, and organelles such as mitochondria [32]. Inactive white matter lesions become more abundant in late phases with few or no microglia and macrophages, decreased inflammation, and axonal damage [18, 31]. Remyelinated plaques contain few macrophages, and axons with thinner myelin sheaths [18]. In cortical tissue, magnetic resonance imaging indicates that demyelination occurs in early-stage MS [35]. Cortical lesions in MS have been more difficult to visualize and are associated with progression and disability [12, 35]. Given the complex evolution of demyelination in MS, a robust method for studying global molecular changes in brain tissue would be of great value to better understand biochemical changes associated with disease progression.

Fourier-transform infrared (FTIR) spectroscopy is a non-destructive technique that can inform on biomolecules including lipids, proteins, phosphate, and carbohydrates [3]. Several studies have demonstrated the utility of infrared spectroscopy for the analysis of brain tissue [41]. For instance, Noreen and colleagues utilized FTIR spectroscopy to examine collagen content in brain gliomas. The authors were able to use chemometric approaches to discriminate tumor brain samples from healthy controls. Furthermore, they found that solid and diffuse tumors could be distinguished with respect to the secondary structure profiles of fibrillar and non-fibrillar collagens, respectively [41]. In a study by Gallant et al., infrared microspectroscopy was used to analyze creatine deposits in transgenic amyloid precursor protein mice [20]. They identified sharp spectral bands in the brain tissue of transgenic mice that aligned with that of pure creatine suggestive of altered bioenergetics. Extensive creatine load was in all transgenic mice, which were significantly lower or absent in control mice. Moreso, the authors showed that similar spectral signatures could be detected in human Alzheimer's brain tissue, which was far less in non-demented tissue [20]. Miller and colleagues demonstrated the utility of correlating infrared microspectroscopy with that of X-ray fluorescence imaging in Alzheimer's disease brain tissue [39]. They detected elevated β-sheet content in amyloid plaques using infrared spectroscopy, which colocalized with zinc and copper as detected by X-ray fluorescence imaging suggesting a potential role for metal ions in the formation of amyloid plaques [39]. To date, very few studies have used FTIR spectroscopy to investigate changes in human MS brain tissue [14, 33]. An early study by Choo and colleagues reported that white and gray matter and chronic plaques could be discriminated by their lipid composition and water content [14]. LeVine et al. identified a reduction in lipids and an increase in oxidative stress signatures in white matter [33]. Additional studies utilized biofluids derived from MS patients and detected metabolic and protein structural changes in blood [15, 29]; and decreased lipids, lipid chain length, proteins, and lipid saturation in cerebral spinal fluid of relapse-remitting MS patients [60]. Similarly, a study using an experimental autoimmune encephalomyelitis mouse model of MS found decreased lipid ester carbonyl groups in lesions [25]. While these studies provide useful insights into MS-related biomolecular changes, alterations occurring during different stages of demyelinating activity have not been thoroughly investigated using FTIR spectroscopy. In this study, we use brain tissue from a cohort of well characterized MS patients. Lesions in white matter were staged by their demyelinating activity. We also interrogated changes in the cortex and cortical lesions of MS. Our results demonstrate extensive biomolecular changes of lipids, proteins, phosphate, and carbohydrates in MS brain tissue, which likely reflects the complex dynamic evolution of lesions and pathological changes within diseased tissue.

Materials and methods

Inclusion criteria and sample characterization

This study was approved by the Mayo Clinic institutional review board (Rochester, MN). All tissue was obtained from the Department of Neurology at Mayo Clinic (Rochester, MN). We used formalin-fixed paraffin-embedded (FFPE) autopsy and biopsy brain tissue from patients diagnosed with MS or control individuals without known neurological disorders (Supplemental Table 1). Diagnosis of MS was confirmed by a certified neurologist according to McDonald or Poser criteria [37, 47]. We included 10 control autopsy cases, and 18 autopsy and 6 biopsy MS cases (Supplemental Table 1). A summary of the available clinical information for MS patients is presented in Supplemental Table 2. The median disease duration was 30 days (range of 10 days to 1.8 months) for MS biopsy cases and 11.5 years for MS autopsy cases (range of 3 weeks to 28 years). The median age at biopsy or death was 55.2 ± 16.0 years. Eight MS patients had RRMS, 6 SPMS, 6 monophasic, 1 PPMS, 1 silent MS, and 2 cases had no available information.

Immunohistochemistry and pathological classification

All FFPE tissue was sectioned at the Mayo Clinic Pathology Research Core (Rochester, MN). Consecutive tissue sections were used for immunochemistry staining and FTIR spectroscopy. To determine demyelinating activity,

5 µm thick FFPE sections were stained with hematoxylin and eosin (H&E), and Luxol fast blue and periodic acid Schiff (LFB/PAS). Immunohistochemistry was performed with EnVisionTM FLEX immunohistochemistry system (DAKO), using primary antibodies against neurofilament (1:800, steam antigen retrieval with citric acid buffer pH 6.0, DAKO, Denmark), myelin proteolipid protein (PLP, 1:500, Serotec, Oxford, UK), myelin associated glycoprotein (MAG, 1:1000, Abcam), myelin oligodendrocyte glycoprotein (MOG, 1:1000, Abcam), and CD68 KP1 (1:100, DAKO, Denmark). Demyelinating activity was staged by the presence of specific myelin degradation products within myeloid cells as previously described [6, 44]. Briefly, early active demyelination presented with myelin-laden macrophages expressing both minor and major myelin proteins. Late active demyelination exhibited macrophages immunoreactive for major myelin proteins only. Early and late active lesions were grouped for analysis and referred to as 'active' in this study. Inactive demyelination lacked myelin-laden macrophages. Periplaque white matter (PPWM) denoted non-demyelinated white matter surrounding the demyelinating plaque. Remyelination was defined as focal areas with reduced myelin density and thin myelin sheath. Fully remyelinated plaques are called shadow plaques. However, partially and fully remyelinated plaques are referred to as 'remyelination' in this study. Normal appearing white matter (NAWM) was defined as non-demyelinated white matter far away from the demyelinating plaques. Subpial (SP) cortical lesions were defined as confluent demyelination extending from the pia to the deeper cortex.

Fourier-transform infrared spectroscopy

Five µm thick tissue sections were mounted onto BaF_2 slides (Alkor Technologies, Saint Petersburg, Russia). The mounted tissue was incubated at 65 °C for 60 min to melt and remove most of the paraffin. Residual paraffin was removed using standard xylene and ethanol rinses. Deparaffinized tissue sections were then stored in a desiccator for a minimum of 24 h prior to scanning. Fourier-transform infrared spectroscopy was performed on an Agilent Cary 620 microscope coupled with Cary 670 spectrometer equipped with a 128 × 128 focal plane array detector (Agilent, Santa Clara, CA, USA). We used the transmission mode with a spectral resolution of 8 cm^{-1} and spatial resolution of 20 µm within the 3900–950 cm^{-1} range. Spectral data was collected with 48 scans per pixel. Background spectra was collected from a clean surface of the BaF_2 slide, which was used to subtract atmospheric and beam current changes from the acquired data. The system was purged using a nitrogen stream during data acquisition. Data acquisition was performed using Agilent Resolution Pro software (v5.2) (Agilent, Santa Clara, CA, USA). The tissue area and total number of ROIs scanned can be seen in Supplemental Table 3.

Hyperspectral images and pre-processing of spectra

Hyperspectral images were generated in Resolution Pro software using the average of all raw spectra for the following regions: amide I, 1700–1600 cm^{-1}; asymmetric phosphate, 1280–1200 cm^{-1}; and total lipids, 3000–2800 cm^{-1}. Pre-processing of spectral data was performed using Spectroscopy package (v0.4.9) developed for the Quasar Orange platform (v3.29) running on Python (v3.11) [16, 56, 57]. The raw spectra were cropped to 3800–950 cm^{-1}. The spectral region corresponding to CO_2 (2400–2250 cm^{-1}) was removed. The spectra were baseline corrected using the rubber-band method. Baseline-corrected spectra underwent PCA denoising using 30 components. The spectra were then processed using unsupervised k-means clustering (8 clusters) to help identify and remove background and artifacts. The spectra were cropped from 3700–2400 cm^{-1} and 1800–1050 cm^{-1} followed by baseline correction using the rubber band method. The spectra were integrated and averaged using the regions listed in Table 1. Ratios were quantified similarly as seen in [27, 51]. However, rather than using a single peak intensity, we used the average integrated area under the absorbance spectra for the corresponding regions listed in Table 1. Regions of interest (ROI; e.g., lesions, white matter, cortex, etc.) were selected based on histopathology maps. The absorbance spectra for each ROI were then averaged. Individuals presenting with more than one ROI of the same classification (e.g., multiple active lesions within the same individual) were averaged into a single value (Supplemental Table 3). For second derivative analysis, the absorbance spectra were processed using the Savitzky-Golay method (window size = 5 and polynomial order = 2) followed by vector normalization and averaged.

Data analysis

Significant changes between groups of the integrated spectra and ratios were detected using one-way ANOVA post hoc Tukey test in GraphPad Prism (v9). Bar plots and line graphs representing the absorbance and second derivative spectra, respectively, were generated using GraphPad Prism. Multivariate analysis was carried out in R (v4.1.1) using the mixOmics package (v6.18.1) [50]. The average second derivative spectra from 3000–2800 cm^{-1} and 1800–1050 cm^{-1} were used for sparse partial least squares-discriminant analysis (sPLS-DA). The sPLS-DA models were optimized using fivefold cross-validation with 100 repeats stratified so each fold contains nearly equal amounts of samples from each group. For the

Table 1 Spectral region assignments

Peak frequency (cm^{-1})	Designation	Proposed assignment
3027–3000	Total olefin	= CH stretching, unsaturated lipids
3000–2800	Total lipids	CH_2 and CH_3 stretching
2970–2945	Lipids	CH_3 asymmetric stretching, mainly lipids
2930–2905	Lipids	CH_2 asymmetric stretching, mainly lipids
2880–2860	Lipids	CH_3 symmetric stretching, mainly lipids
2860–2840	Lipids	CH_2 symmetric stretching, mainly lipids
1755–1715	Total carbonyl	C = O stretching
1700–1600	Total amide I	C = O, and C-N stretching, N–H bending vibrations of proteins
1670–1650	Amide I	Proteins, mainly α-helix
1650–1635	Amide I	Proteins, unordered structures
1635–1620	Amide I	Proteins, β-sheet structures
1280–1200	Phosphate	PO_2- asymmetric stretching vibrations of RNA, DNA, and phospholipids
1175–1145	Carbohydrates	Glycogen, collagen, amino acids, ribose

white matter, three components with 5, 5, and 10 latent variables were used. Likewise, the cortex sPLS-DA model used three components with 60, 9, and 80 latent variables. The area under the receiver operating characteristic (AUROC) curve was averaged over the cross-validation process using a one-vs-all comparison [50]. Both the sPLS-DA plot and AUROC curve were generated using the mixOmics package.

Results

Fourier transform infrared spectroscopy is sensitive to different stages of demyelination in MS brain tissue

We used FTIR spectroscopy of MS lesions to get new insight into biomolecular changes at various stages of demyelination that is not routinely detected by standard immunohistopathological approaches. Brain tissue sections of MS patients containing active, inactive, and remyelinated lesions were scanned by FTIR spectroscopy (Supplemental Table 1 and Fig. 1). Routine immunohistochemistry of myelin in control and MS tissues are depicted in Fig. 1A–D. Corresponding hyperspectral images of total lipids (Fig. 1E–H) and amide I (Fig. 1I–L) indicate reduced lipids and amides in MS tissue with lesions being the most affected compared to controls.

Next, we sought to determine if the spectral profiles detected at various stages of demyelination were unique to the MS brain tissue. The absorbance profiles were converted to second derivative spectra and analyzed by sparse partial least squares-discriminant analysis (sPLS-DA) (Fig. 2). The sPLS-DA and AUROC plots (Fig. 2A, B, respectively) indicate good separation between the white matter of controls, NAWM, and demyelinated plaques in MS brain tissue. Thus, FTIR spectroscopy and multivariate analysis suggest that MS brain tissue exhibits its unique spectral features that may inform on distinct biomolecular changes occurring at different stages of demyelination.

Lipid loss in the white matter reflects demyelinating activity and altered membrane organization

To evaluate biomolecular alterations at various stages of demyelination in MS lesions, we interrogated spectral markers characteristic for lipids, proteins, phosphate, and carbohydrates. To inform on total lipid content, we integrated the area under the absorbance spectrum from 3000–2800 cm^{-1} (Fig. 3A). The integrated absorbance profiles of total lipids were reduced in MS brain tissue of inactive plaques (p-value < 0.0001), active lesions (p-value = 0.0009), and remyelinated regions (p-value = 0.0013) when compared to control white matter (Fig. 3B). A significant increase in total lipids was observed in remyelinated plaques when compared to inactive plaques (p-value = 0.0282; Fig. 3B). Unsaturated lipids were detected by integrating the olefinic peak between 3027–3000 cm^{-1} [8, 48]. A significant decrease in the total olefinic lipid content was detected in inactive plaques when compared to active lesions, PPWM, NAWM, and control white matter (p-value = 0.0003, p-value < 0.0001, p-value < 0.0001, and p-value < 0.0001, respectively; Fig. 3C). The total carbonyl ester (C = O) content was integrated between 1755–1715 cm^{-1} and was significantly decreased in inactive (p-value < 0.0001) and active (p-value = 0.0008) lesions when compared to control white matter (Fig. 3D). Similarly, the carbonyl ester content in active and inactive lesions was significantly reduced when compared to NAWM (p-value = 0.0008

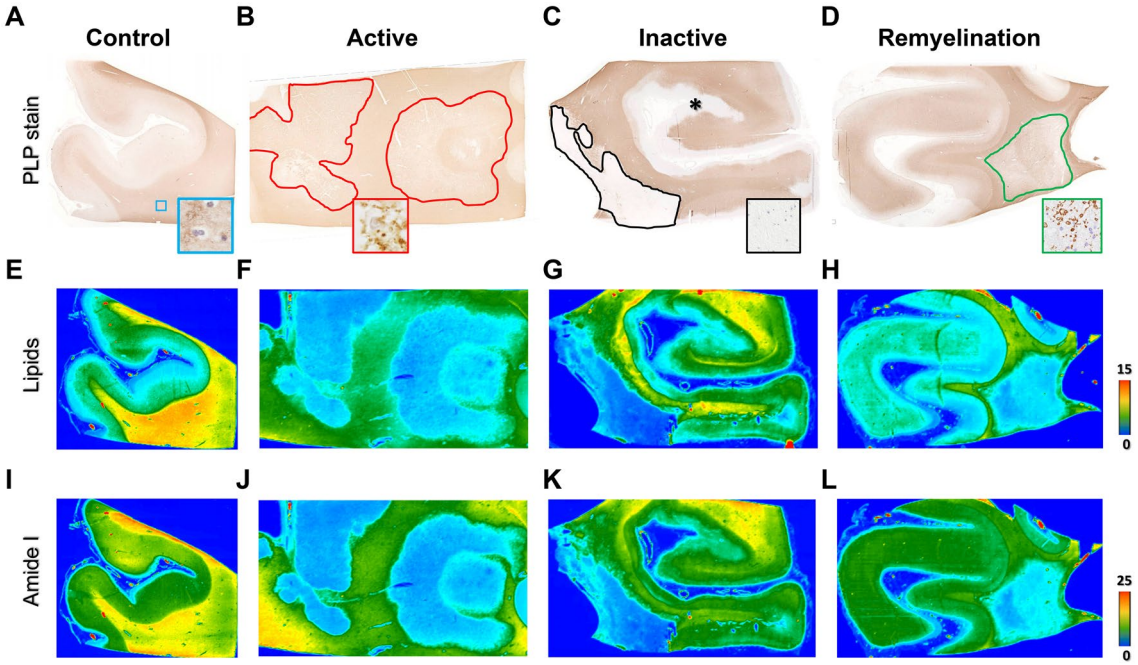

Fig. 1 Hyperspectral imaging readily detects regions of demyelinating activity in MS brain tissue. **A–D** Immunohistochemical staining of myelin proteolipid protein (PLP). Active demyelination, inactive demyelinated, and remyelinated regions in MS brain tissue are outlined in red, black, and green, respectively. Hyperspectral images of **E–H** total lipids and **I–L** amide I were generated using the absorbance profiles from 3000–2800 cm^{-1} and 1700–1600 cm^{-1}, respectively. Scale bars are indicative of abundance as determined by absorbance profiles

and < 0.0001, respectively) and PPWM (p-value = 0.0045 and 0.0002, respectively) regions (Fig. 3D). To further characterize biological changes occurring in MS white matter brain tissue, we evaluated ratios that reflect previously reported biomolecular alterations in tissue, cells, and biofluids. The ratio of total olefin to total lipids was significantly increased in inactive plaques (p-value < 0.0001), active lesions (p-value < 0.0001), remyelinated regions (p-value = 0.0004), and PPWM (p-value = 0.0093) when compared to control white matter suggesting that the relative amount of unsaturated lipids is greater in MS brain tissue (Fig. 3E) [2]. Lipid chain length was assessed using the ratio of total CH_2 to total lipids [11]. Compared to controls, we detected significant decreases in the length of lipid chains in inactive plaques (p-value < 0.0001) and active lesions (p-value < 0.0001) (Fig. 3F). The lipid methyl content was measured using the ratio of total CH_3 to total lipids [11]. In MS brain tissue, we observed a significant increase of the relative lipid methyl content of inactive plaques (p-value = 0.0193) when compared to controls (Fig. 3G). Carbonyl ester content was assessed by the ratio of carbonyl ester to total lipids [2], which revealed a significant decrease in active lesions when compared to PPWM (p-value = 0.047), and NAWM (p-value = 0.0115) (Fig. 3H). To further characterize biomolecular changes in lipids of MS white matter brain tissue, we evaluated the second derivative spectra to resolve peaks corresponding to asymmetric CH_3, asymmetric CH_2, symmetric CH_3, and symmetric CH_2 (Fig. 3I). We detected shifts in the asymmetric and symmetric CH_2 peaks towards lower wavenumbers in all MS white matter tissues with the greatest change in inactive plaques indicating increased lipid order and reduced acyl chain flexibility (Fig. 3I) [10, 48]. Collectively, these data show alterations in the content and structure of lipids in MS brain tissue, which affects inactive lesions most severely with few to no changes in PPWM and NAWM when compared to control individuals.

White matter demyelination is accompanied by protein reduction and altered secondary structures

Next, we interrogated the amide I region (1700–1600 cm^{-1}) to look for changes in the content and structure of proteins (Fig. 4A). Integration of the absorbance spectra shows a significant reduction of protein content in active lesions (p-value = 0.019), inactive plaques (p-value < 0.0001), and remyelinated regions (p-value = 0.0032) when compared to control white matter (Fig. 4B). Compared to NAWM and PPWM, significant reductions in protein abundance were detected in inactive lesions (p-value < 0.0001

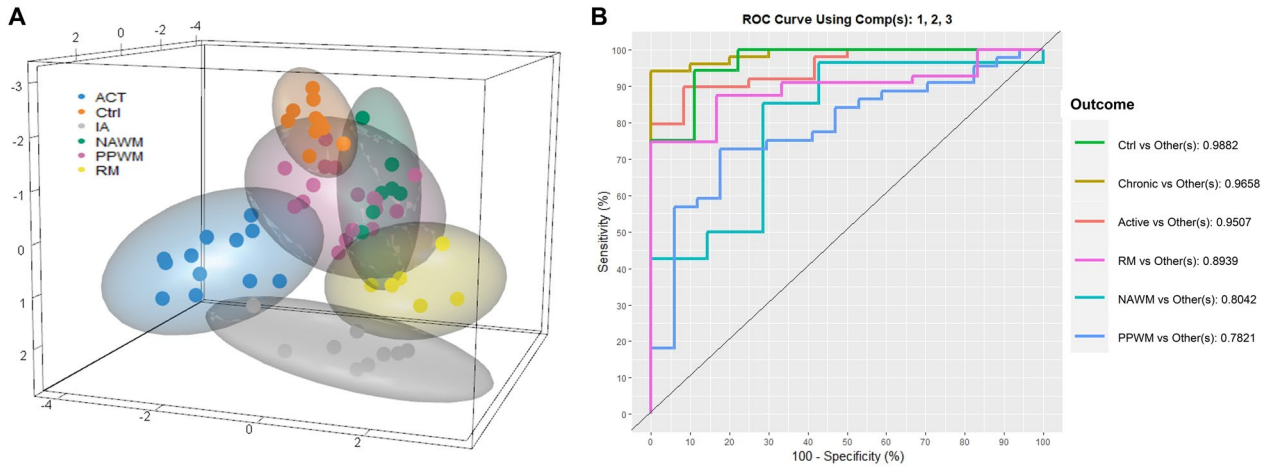

Fig. 2 Multivariate analysis of the second derivative spectra distinguishes between MS demyelinating stages in white matter. The average second derivative spectra from active and inactive lesions, remyelinated regions, periplaque white matter (PPWM), normal appearing white matter (NAWM), and control tissue were used for PLS-DA. **A** A PLS-DA plot using three components with 5, 5, and 10 variables selected. Ellipses depict the 95% confidence interval for each group. **B** The AUROC curve indicates good separation of different demyelinating stages in MS and control white matter

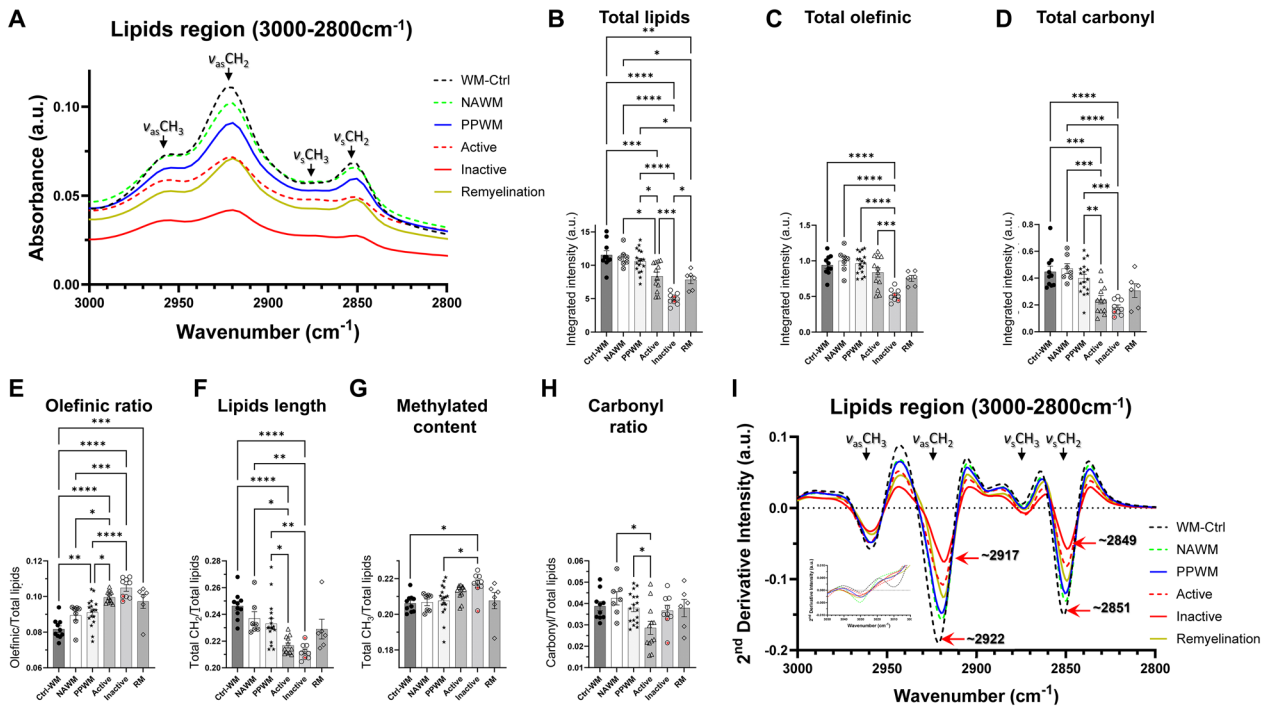

Fig. 3 Lipid loss and perturbed membrane organization in demyelinated MS white matter. **A** The average absorbance spectra of total lipids detected in MS and control white matter brain tissue. Relevant spectral bands are indicated. The integrated area under the absorbance spectra for **B** total lipids, **C** total olefinic, and **D** total carbonyl ester. **E–H** Quantitative ratios of **E** total olefin/total lipids, **F** total CH_2/total lipids, **G** total CH_3/total lipids, and **H** total carbonyl ester/total lipids utilizing the integrated absorbances for the respective regions. **I** The corresponding second derivative of the absorbance spectra. Red arrows indicate peak shifts. The inset shows the olefinic region from 3050–3000 cm^{-1}. Significance was detected using one-way ANOVA with post hoc Tukey test (* $p < 0.05$, ** $p < 0.01$, and *** $p < 0.001$, and **** $p < 0.0001$). Red stars indicate inactive lesions that were detected in acute cases. Integrated regions were as follows: asymmetric CH_3, 2945–2970 cm^{-1}; asymmetric CH_2, 2905–2930 cm^{-1}; symmetric CH_3, 2860–2880 cm^{-1}; symmetric CH_2, 2840–2860 cm^{-1}; and total lipids, 3000–2800 cm^{-1}. Total CH_2 and CH_3 is the summation of asymmetric and symmetric peaks

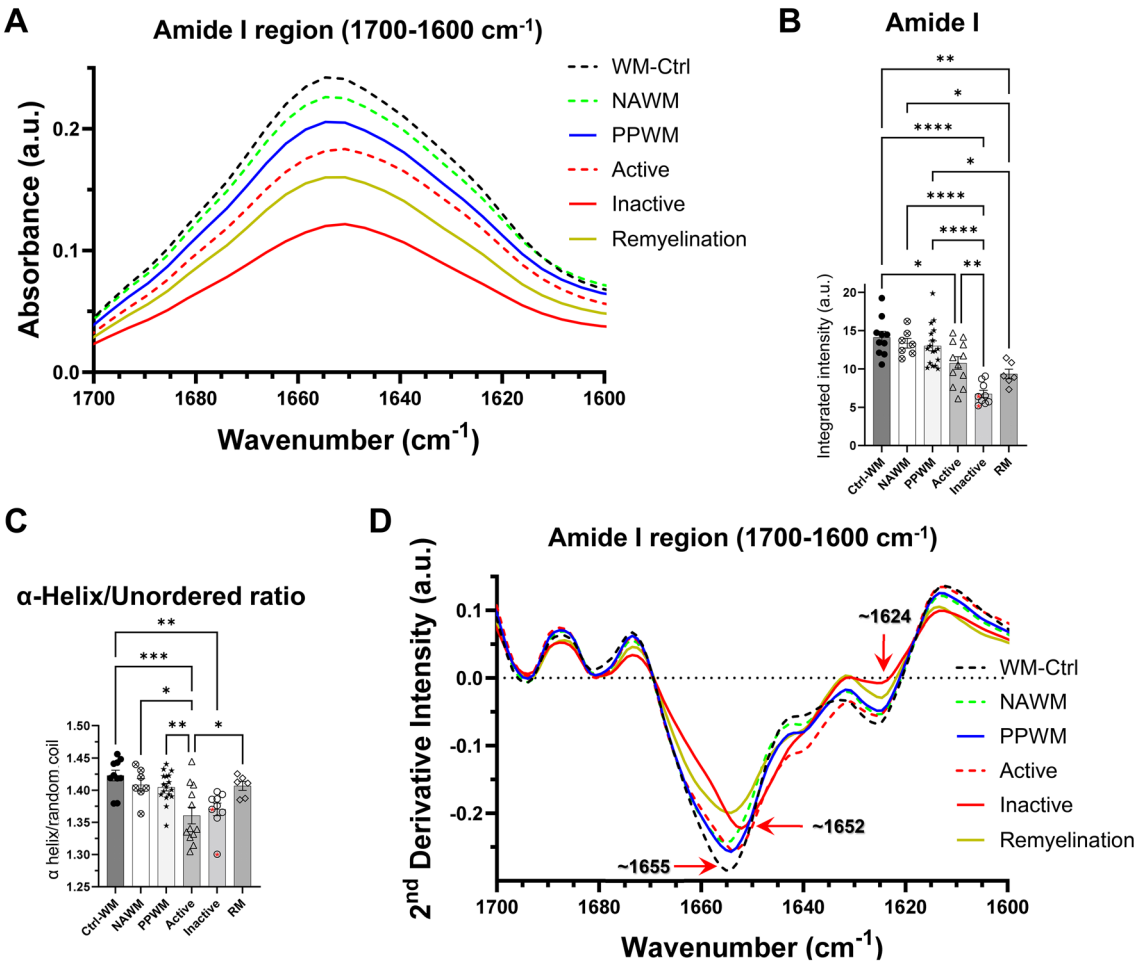

Fig. 4 Demyelinated MS brain tissue has reduced protein abundance and altered secondary structures. **A** The average absorbance profile of control and MS white matter tissue. **B** The integrated area under the absorbance spectra for amide I (1700–1600 cm^{-1}). **C** The ratio of α-helixes to unordered protein structures. **D** The second derivative spectra of the amide I absorbance profiles. Peak shifts are indicated. Significance was detected using one-way ANOVA with post hoc Tukey test (* $p < 0.05$, ** $p < 0.01$, and *** $p < 0.001$, and **** $p < 0.0001$)

and < 0.0001, respectively) and remyelinated plaques (p-value = 0.0378 and 0.0212, respectively; Fig. 4B). We found significant decreases in the ratio of α-helix to unordered structures in active and inactive lesions (p-value = 0.0002 and 0.0047, respectively) compared to control white matter (Fig. 4C). Analysis of the second derivative spectra for the amide I region revealed clear differences in peak intensities and protein order between the various demyelinating stages of MS lesions (Fig. 4D). Interestingly, inactive plaques were the only group to have a major shift in their α-helix region towards lower wavenumbers (Fig. 4D). The appearance of a shoulder near 1640 cm^{-1} was apparent in MS tissue and was most prominent in active lesions (Fig. 4D). Additionally, β-sheet structures near 1630 cm^{-1} appear to be decreased in MS tissue with inactive plaques having the most apparent reduction (Fig. 4D). These findings support the notion that protein content is reduced in demyelinated MS brain tissue and are accompanied by altered secondary structures of proteins.

Phospholipid disorder is accompanied by metabolic changes in the white matter

Mitochondrial injury and accompanying energy deficiency and are well associated with MS [32]. To gain additional insight into potential energy failure and cellular dysfunction, we examined peaks between 1300–1100 cm^{-1}, which are closely associated with phosphate and carbohydrates (Fig. 5A) [36]. Integration of the asymmetric phosphate peak between 1280–1200 cm^{-1} revealed a significant phosphate decrease in active plaques (p-value = 0.0018) and inactive lesions

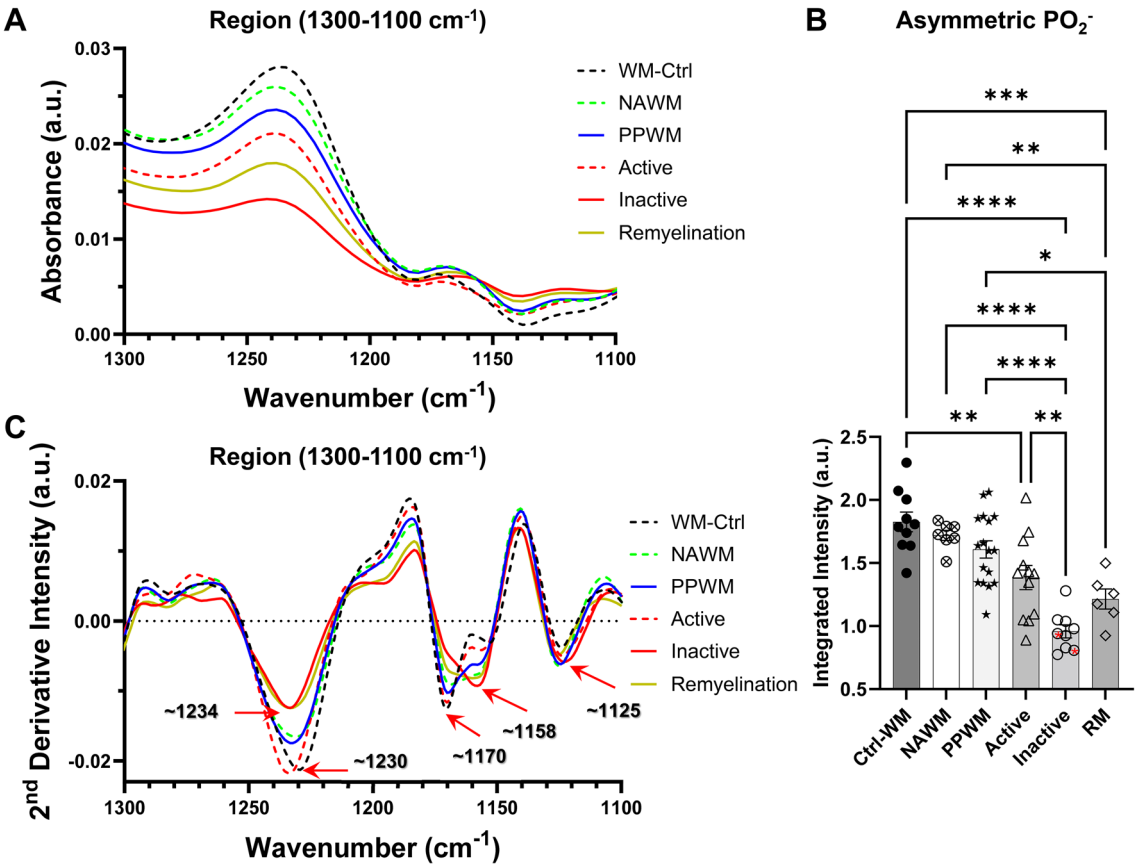

Fig. 5 Reduced asymmetric phosphate and possible metabolic rearrangements in demyelinated MS white matter. **A** The average absorbance spectra of MS and control white matter brain tissue. **B** The integrated absorbance of the asymmetric phosphate band (1280–1200 cm^{-1}). **C** The average second derivative of the absorbance spectra. Peak shifts and relevant bands are indicated by arrows. Significance was detected using one-way ANOVA with post hoc Tukey test (* $p < 0.05$, ** $p < 0.01$, and *** $p < 0.001$, and **** $p < 0.0001$)

(p-value < 0.0001) when compared to controls (Fig. 5B). The loss of asymmetric phosphate in lesions was partially recovered in remyelinated plaques but remained significantly decreased when compared to controls (Fig. 5B). Interestingly, second derivative analysis shows no change in the peak intensity of asymmetric phosphate in active lesions relative to controls (Fig. 5C). We also observed a shift of the asymmetric phosphate peak to higher wavenumbers in MS white matter compared to control white matter (Fig. 5C). The second derivative spectra further revealed three peaks near 1170 cm^{-1}, 1158 cm^{-1}, and 1125 cm^{-1} in the white matter of controls and MS tissue, which have been associated with amino acids, glycogen, and ribose, respectively (Fig. 5C) [5, 19]. Intriguingly, the peak near 1158 cm^{-1} has an increase in inactive plaques, remyelinated plaques, and NAWM followed by PPWM in comparison to active lesions and control white matter (Fig. 5C). Taken together, these results suggest a decrease of phosphate in demyelinated MS lesions, which may be accompanied with altered metabolic activity.

Biochemical changes in MS cortex

Cortical demyelination has been linked to cognitive impairment, disease progression, and atrophy in MS [35]. However, the relationship between demyelination in the cortex and biomolecular alterations in MS remain elusive. Therefore, we used FTIR spectroscopy to gain insight into biochemical changes occurring during cortical demyelination. Histopathological maps and hyperspectral images of total lipids (3000–2800 cm^{-1}) and amide I (1700–1600 cm^{-1}) are in close agreement revealing the ability of FTIR to detect cortical lesions (Fig. 6A, B, C, respectively). Unsaturated lipids (olefin/total lipids) are significantly increased in both periplaque cortex (PP-Ctx, p-value = 0.0168) and subpial cortical lesions (SP, p-value = 0.0208) when compared to control cortex (Ctrl-Ctx; Fig. 6D). Acyl chain length (total CH_2/total lipids) was significantly decreased in the PP-Ctx (p-value = 0.0113) and SP lesions (p-value = 0.0058; Fig. 6E) when compared to the normal appearing cortex (NA-Ctx). Analysis of the amide I region

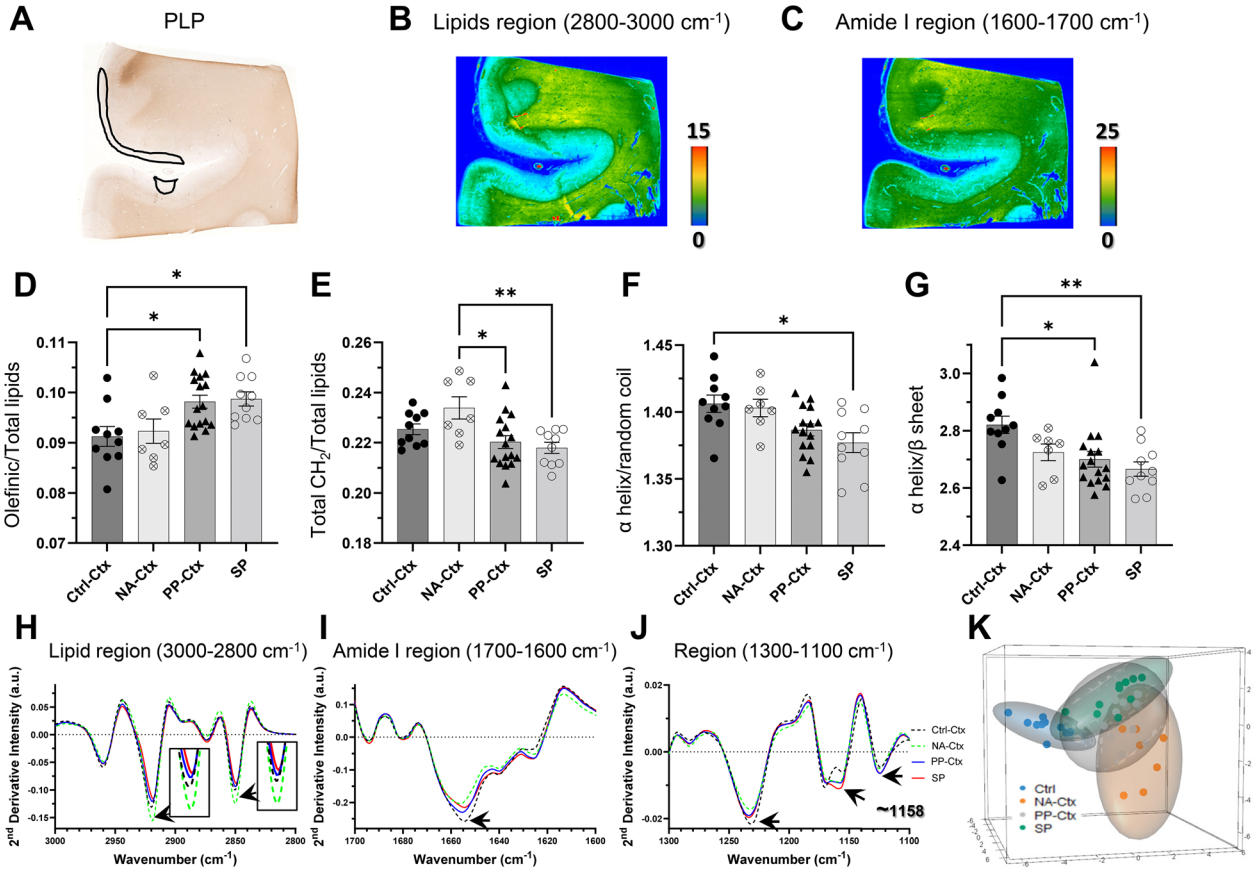

Fig. 6 Biomolecular alterations detected in MS cortex. **A** Myelin staining as detected by PLP1 in MS brain tissue. The black outline shows regions of demyelination in the cortex. **B, C** Hyperspectral images of the tissue seen in **A** using the abundance of total lipids and amide I, respectively. **D–G** Quantitative ratios using the integrated area under the absorbance spectra. **H–J** The average second derivative spectra of total lipids, amide I, and phosphate and carbohydrate regions, respectively. **K** The second derivative spectra of MS and control cortex was analyzed using sPLS-DA. The first three components with 60, 9, and 80 variables were used. The ellipses indicate the 95% confidence interval. Integrated regions: α-Helix, 1670–1650 cm^{-1}; β-Sheets, 1635–1620 cm^{-1}; Total CH_2, 2930–2905 cm^{-1} + 2860–2840 cm^{-1}; Total lipids, 3000–2800 cm^{-1}; Total olefinic, 3027–3000 cm^{-1}; and unordered structures, 1650–1635 cm^{-1}. Significance was detected using one-way ANOVA with post hoc Tukey test (* $p < 0.05$ and ** $p < 0.01$)

identified two ratios that were significantly reduced in cortical lesions when compared to control cortex. The ratio of α-helix to unordered structures (1670–1650 cm^{-1}/1650–1635 cm^{-1}) was significantly reduced in cortical lesions (p-value = 0.0108), while the ratio of α-helix to β-sheets (1670–1650 cm^{-1}/1635–1620 cm^{-1}) was reduced in the periplaque cortex and cortical lesions (p-value = 0.0164 and p-value = 0.0044, respectively) when compared to control cortex (Fig. 6F, G). Among 24 MS cases used for cortical analysis six have confounding neurodegenerative pathology, however, the inclusion or exclusion of those cases did not influence the conclusions (see Supplemental Fig. 1).

Analysis of the second derivative spectra revealed several changes in the MS cortex when compared to control tissue (Fig. 6H–J). Within the total lipid region (3000–2800 cm^{-1}), profound peak intensity decreases in the asymmetric and symmetric CH_2 were observed for Ctrl-Ctx, PP-Ctx, and SP lesions when compared to NA-Ctx (Fig. 6H). In the amide I region (1700–1600 cm^{-1}), the peak intensity of the α-helical region of MS cortical tissue was decreased when compared to Ctrl-Ctx. Additionally, MS cortical tissue had a shift in the α-helix to higher wavenumbers compared to Ctrl-Ctx (Fig. 6I). We observed reduced asymmetric phosphate peak intensity in MS cortex compared to controls in the region 1300–1100 cm^{-1} (Fig. 6J). Interestingly, similar to observations in MS white matter, we observed a substantial increase in the peak intensity at 1158 cm^{-1} of MS cortex when compared to control tissue (Fig. 6J). Analysis of the second derivative spectra using sPLS-DA show good separation of the Ctrl-Ctx spectra from MS cortex (Fig. 6K). The PP-Ctx and SP lesions had the greatest overlap (Fig. 6K), however, the AUROC curve confirms reasonable separation between

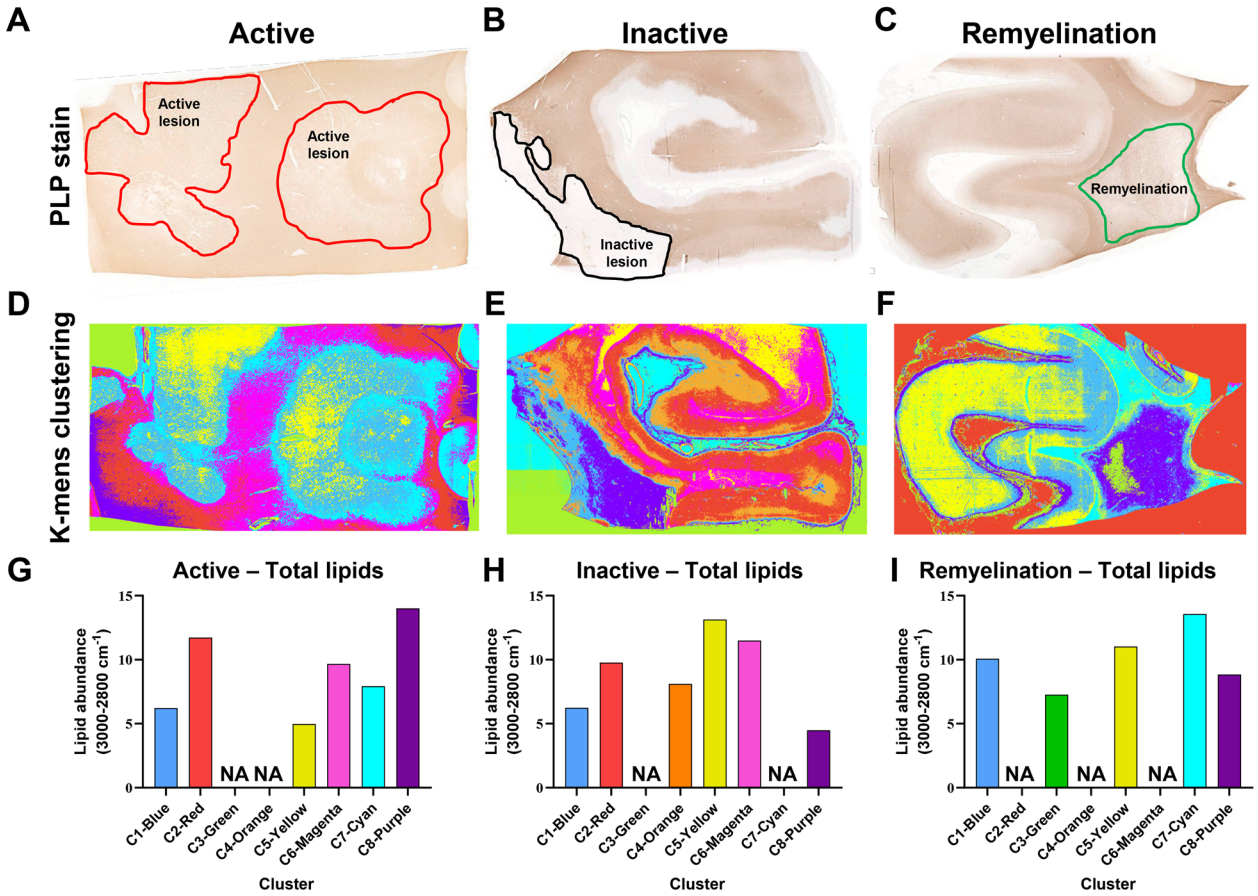

Fig. 7 Unsupervised clustering detects heterogeneity in MS brain lesions. **A–C** Immunohistochemical staining of myelin using PLP1. Active lesions, inactive plaques, and remyelinated regions are outlined in red, black, and green, respectively. **D–F** Unsupervised k-means clustering of MS brain tissue seen in **A**–**C** using the absorbance spectra as detected by FTIR spectroscopy. A total of eight clusters were used. **G–I** The average total lipid abundance (3000–2800 cm^{-1}) for each respective cluster as shown in D-F. The NA (not applicable) corresponds to clusters designating background

the groups (AUROC > 0.7 for all groups, Supplemental Fig. 2). Taken together, FTIR spectroscopy suggest that alterations in lipids, proteins, phosphate, and carbohydrates are present in the MS cortex revealing biomolecular changes associated with cortical demyelination.

Biomolecular heterogeneity in MS lesions detected by k-means clustering

Lesion heterogeneity in MS is well established [34]. Changes in the biochemical properties of MS brain tissue may impact the function of molecular and cellular processes involved in the pathophysiology of MS. Using FTIR spectroscopy and unsupervised machine learning, we studied three representative MS brain tissues sections containing active, inactive, and remyelinated plaques to gain insight into potential biomolecular heterogeneity (Fig. 7). Routine PLP immunohistochemistry of MS brain tissue identifies active, inactive, and remyelinated plaques (Fig. 7A–C, respectively). Fourier transform infrared spectroscopy and unsupervised clustering reveals changes not readily detected by PLP staining (Fig. 7D-F). In active lesions, three clusters were identified within the plaque and three were identified outside of the lesion (Fig. 7D). Integration of the total lipid region (3000–2800 cm^{-1}) indicates variable loss of lipids within the plaques when compared to surrounding white matter tissue (Fig. 7G). In the inactive lesion (Fig. 7E, H) and remyelinated plaques (Fig. 7F, I) two clusters were revealed in which the lipid content was lower. The remyelinated plaque was bordered by a white matter rim characterized by a lipid content more similar to that of the cortex, but lower than that of the PPWM (Fig. 7F, I). Overall, these results demonstrate the ability of FTIR spectroscopy to detect underlying patterns of biochemical changes that are not readily detectable by routine histopathology.

Discussion

The ability to interrogate the heterogeneity and dynamic nature of MS lesions in various demyelinating stages will provide us with greater opportunity to identify new therapeutic targets. Halting or even reversing progression in MS will require a holistic understanding of changes occurring in MS lesions. This study demonstrates the ability of FTIR spectroscopy to identify biochemical changes of lipids, proteins, phosphate, and carbohydrates in MS brain tissue. We further establish the use of multivariate analysis to discriminate between lesions at different stages of demyelinating activity. This study introduces a framework to characterize features of MS lesions not identifiable with routine histopathology, which should help enhance our understanding of disease progression in MS.

We found that inactive plaques in MS white matter showed the greatest changes when compared to control white matter. Similar changes were detected in active lesions, but to a lesser extent. Likewise, remyelinated plaques were not as impacted as inactive plaques, which may reflect structural recovery within shadow plaques. As expected, a significant decrease in total lipids was detected in all MS lesions when compared to controls. Utilizing quantitative ratios previously described in the literature, we were able to gain additional insight into lipid changes occurring in MS brain tissue. The degree of lipid unsaturation was assessed by the olefinic region [8, 48], and only showed a significant decrease in MS inactive plaques when compared to control white matter. However, when normalized to total lipid content a significant increase in unsaturated lipids were detected in the PPWM, active lesions, inactive lesions, and remyelinated plaques. This suggests that high levels of unsaturated lipids are present in MS brains increasing the susceptibility to attack by reactive oxygen species [53, 60]. Peroxidation of unsaturated lipids has been linked to the pathogenesis of neurodegenerative diseases [49], and Haider and colleagues demonstrated increased oxidized DNA and lipids in active and inactive lesions, PPWM, and NAWM of MS brain tissue using immunohistochemical markers of oxidation [22]. Products of lipid peroxidation, including malondialdehyde, have been previously described in MS active lesions, inactive plaques, and NAWM [22]. We also assessed the length of the lipid acyl chain as a marker of lipid degradation [11], and found significant length decreases in active and inactive lesions when compared to controls [11]. Furthermore, we detected a significant increase in the lipid methyl content of inactive plaques, which has been associated with increased lipid peroxidation as degradation products will have methyl groups albeit shorter acyl chains [1, 11]. Interestingly, despite having the most profound loss of total lipids, inactive white matter lesions still show a relative increase in unsaturated and methylated lipids, as well a decrease in lipid length, showing that while long-standing oxidative damage is a hallmark of inactive lesions, they are still susceptible to new damage by reactive oxygen species. The lipid changes we report may also suggest that membrane structure, stability, permeability, and fluidity are affected impacting cellular shape, signaling, and function [9, 30, 38, 59]. This is highlighted by band shifts in the second derivative spectra of asymmetric/symmetric CH_2 in MS white matter suggestive of increased lipid order with decreasing acyl chain flexibility [10, 48], which may have a major impact on myelin adhesion and permeability resulting in demyelination [43]. In vitro models of myelin membranes suggest that altered lipid composition and abundance of myelin basic protein can result in structural instabilities [54]. Modified lipid compositions in myelin membranes may be related to changes in fluidity and lipid domain distributions, which can further alter myelin basic protein adhesion and promote abnormal structures that may increase exposure to immune system attacks [54]. Thus, changes in the lipid spectra of MS brain tissue could be reflecting changes in myelin structure, protein abundance (e.g., myelin basic protein), and/or lipid composition. Future studies correlating MS etiology with spectral changes detected with FTIR spectroscopy could greatly aid in the classification and/or monitoring of therapeutic efficacy in MS.

Similar to lipids, we found that proteins were most heavily perturbed in white matter inactive plaques when compared to controls. Significant protein loss was detected in all demyelinated white matter lesions and were accompanied by secondary structural changes in active and inactive lesions. The second derivative spectra of white matter inactive plaques revealed a shift from 1655 to 1652 cm^{-1} indicative of increasing disordered structures [13, 21, 52]. Compared to control white matter, active lesions had the most prominent appearance of a peak near 1640 cm^{-1}, which is attributed to random coil structures in proteins [52]. As the myelin sheath houses many proteins, it is plausible that demyelination can disrupt the optimal environment for protein folding resulting in perturbed structures [24, 46]. Moreover, endoplasmic reticulum stress, mitochondrial dysfunction, and oxidative stress in MS can all contribute to protein dyshomeostasis [4, 23], which have been previously described in MS blood samples [29], cerebrospinal fluid [60], and brain tissue [33] using FTIR. These findings highlight the utility of FTIR spectroscopy to study pathophysiological changes of proteins in MS.

The asymmetric phosphate band is associated with nucleic acids, phosphorylated proteins, and phospholipids [61]. However, in the white matter, phosphate is

predominately found in phospholipids [7]. Thus, changes detected in the MS white matter asymmetric phosphate likely reflect changes in phospholipids. In MS white matter, we detected significant phospholipid decreases in all stages of demyelinating activity. Moreover, peak shifts in the asymmetric phosphate band to higher wavenumbers in MS white matter tissue suggest a reduction in hydrogen bonding resulting in increased membrane disorder (e.g., packing and fluidity) [28, 55]. Thus, the asymmetric phosphate peak may reflect changes in the abundance and integrity of the myelin sheath in MS brain tissue.

Axonal damage, mitochondrial dysfunction, oxidative stress, and metabolic defects are well described in MS [32]. As mitochondria accumulate oxidative damage, energy metabolism can shift in part due to reduced electron transport chain machinery and mtDNA damage [32]. In our study, we observe a rearrangement in the second derivative spectra of MS white matter near 1158 cm^{-1}, which largely corresponds to glycogen [5]. The glycogen bands in controls and active lesions were similar. Interestingly, increasing intensity of the glycogen band is seen in NAWM, PPWM, and inactive plaques. In the brain, glycogen is primarily stored in astrocytes [42]. Inflammation is most pronounced in active lesions but is seen throughout the course of MS in regions including inactive and remyelinated plaques and NAWM [17]. In astrocytes, mitochondrial metabolic shifts from oxidative phosphorylation to glycolysis has been associated with inflammation [26, 40]. Thus, it is plausible that differential spectral changes in the glycogen band are related to inflammation, mitochondrial dysfunction, and astrocyte activation as it relates to various stages of demyelinating activity.

Pathophysiological mechanisms that result in cortical demyelination in MS remains elusive. However, gray matter atrophy can occur prior to and independently of white matter lesions and serve as a good predictor of neurological disability in MS patients [58]. Thus, mechanisms of cortical demyelination may be different from white matter demyelination in individuals with MS. In our study, we observed some similarities between cortical and white matter lesions including the formation of unsaturated lipids, acyl chain shortening, and protein secondary structural changes. This may suggest that common mechanisms exist affecting both cortical and white matter tissue. One distinct feature in the cortex was an increase in the intensity of symmetric and asymmetric CH_2 and CH_3 seen in the second derivative spectra for normal appearing cortex. As we did not detect significant changes in the abundance of total CH_2 in normal appearing cortex compared to control tissue (Supplemental Fig. 3), intensity alterations in the second derivative may suggest that the structural order of membranes in the normal appearing MS cortex is perturbed when compared to controls [45]. In the white matter, all CH_2 and CH_3 peak intensities were decreased in MS tissue compared to controls. Thus, an increase in intensity in the normal appearing cortex was uniquely suggestive of distinct lipid alterations when compared to white matter tissue.

While current immunohistological approaches are informative and have provided invaluable insight into MS pathogenesis, they can be tedious as numerous stains are needed to obtain a holistic picture. In this regard, FTIR spectroscopy is an ideal platform for the non-destructive analysis of lipids, proteins, phosphate, and carbohydrates in a single analysis. Importantly, FTIR spectroscopy can effectively quantify and detect biochemical and structural changes within MS brain tissue. However, limiting factors exist that require further optimization and/or alternate approaches. For instance, in this study, cortical changes as detected by FTIR spectroscopy were less profound and may not be as suitable to study. Though, optimizing parameters including resolution, sample thickness, acquisition time, and scanning modes may improve sensitivity. Certain elements including metals that do not absorb light will require imaging utilizing alternative platforms such as X-ray fluorescence spectroscopy. As FTIR spectroscopy cannot determine changes in specific molecules, additional targeted analyses may be needed (e.g., metabolomics). However, we were able to utilize the second derivative spectral profiles to demonstrate the feasibility to classify MS lesions using multivariate analysis by their demyelinating activity and differentiate them from control white matter. Using absorbance spectra, we can generate hyperspectral images that not only emphasize the heterogeneity within MS tissue but can be tailored to look for specific spectral markers of interest (e.g., acyl chain length, oxidative stress, structural changes, abundance, etc.). Optimizing these approaches will help advance the classification, staging, and interrogation of MS tissue enhancing our understanding of MS disease mechanisms and potentially identify novel therapeutic targets.

Supplementary Information

The online version contains supplementary material available at https://doi.org/10.1186/s40478-024-01854-4.

Additional file 1.

Author contributions

OG collected and analyzed IR absorption data and contributed significantly to the drafting of the manuscript; JMW performed statistical analysis and contributed significantly to the drafting of the manuscript; YG performed

pathological tissue analysis and mapping; BFP provided expertise with data analysis and interpretations; SDW guided statistical analysis; AKL provided clinical information; CFL conceptualized, supervised, and funded this study. All authors read and approved the final manuscript.

Funding
Center for Multiple Sclerosis and Autoimmune Neurology; Kingsland Foundation.

Declarations

Ethics approval and consent to participate
All patients had provided written informed consent for the use of autopsy and biopsy materials.

Competing interests
The authors declare no conflict of interest.

Received: 10 July 2024 Accepted: 25 August 2024
Published online: 10 September 2024

References

1. Ali MHM, Rakib F, Abdelalim EM, Limbeck A, Mall R, Ullah E, Mesaeli N, McNaughton D, Ahmed T, Al-Saad K (2018) Fourier-transform infrared imaging spectroscopy and laser ablation -ICPMS new vistas for biochemical analyses of ischemic stroke in rat brain. Front Neurosci. https://doi.org/10.3389/fnins.2018.00647
2. Ali MHM, Rakib F, Nischwitz V, Ullah E, Mall R, Shraim AM, Ahmad MI, Ghouri ZK, McNaughton D, Küppers S et al (2018) Application of FTIR and LA-ICPMS spectroscopies as a possible approach for biochemical analyses of different rat brain regions. Appl Sci 8:2436
3. Baker MJ, Trevisan J, Bassan P, Bhargava R, Butler HJ, Dorling KM, Fielden PR, Fogarty SW, Fullwood NJ, Heys KA et al (2014) Using Fourier transform IR spectroscopy to analyze biological materials. Nat Protoc 9:1771–1791. https://doi.org/10.1038/nprot.2014.110
4. Barcelos IP, Troxell RM, Graves JS (2019) Mitochondrial Dysfunction and Multiple Sclerosis. Biology (Basel) 8: https://doi.org/10.3390/biology8020037
5. Bogomolny E, Argov S, Mordechai S, Huleihel M (2008) Monitoring of viral cancer progression using FTIR microscopy: a comparative study of intact cells and tissues. Biochim Biophys Acta (BBA) Gen Subj 1780:1038–1046. https://doi.org/10.1016/j.bbagen.2008.05.008
6. Brück W, Porada P, Poser S, Rieckmann P, Hanefeld F, Kretzschmar HA, Lassmann H (1995) Monocyte/macrophage differentiation in early multiple sclerosis lesions. Ann Neurol 38:788–796. https://doi.org/10.1002/ana.410380514
7. Buchli R, Duc CO, Martin E, Boesiger P (1994) Assessment of absolute metabolite concentrations in human tissue by 31P MRS in vivo. Part I: cerebrum, cerebellum, cerebral gray and white matter. Magn Reson Med 32:447–452. https://doi.org/10.1002/mrm.1910320404
8. Cakmak G, Miller LM, Zorlu F, Severcan F (2012) Amifostine, a radioprotectant agent, protects rat brain tissue lipids against ionizing radiation induced damage: an FTIR microspectroscopic imaging study. Arch Biochem Biophys 520:67–73. https://doi.org/10.1016/j.abb.2012.02.012
9. Cakmak G, Severcan M, Zorlu F, Severcan F (2016) Structural and functional damages of whole body ionizing radiation on rat brain homogenate membranes and protective effect of amifostine. Int J Radiat Biol 92:837–848. https://doi.org/10.1080/09553002.2016.1230237
10. Cakmak G, Zorlu F, Severcan M, Severcan F (2011) Screening of protective effect of amifostine on radiation-induced structural and functional variations in rat liver microsomal membranes by FT-IR spectroscopy. Anal Chem 83:2438–2444. https://doi.org/10.1021/ac102043p
11. Cakmak-Arslan G, Haksoy H, Goc-Rasgele P, Kekecoglu M (2020) Determination of the dose-dependent toxic effects of mad honey on mouse liver using ATR-FTIR spectroscopy. Spectrochim Acta Part A Mol Biomol Spectrosc 228:117719. https://doi.org/10.1016/j.saa.2019.117719
12. Calabrese M, Poretto V, Favaretto A, Alessio S, Bernardi V, Romualdi C, Rinaldi F, Perini P, Gallo P (2012) Cortical lesion load associates with progression of disability in multiple sclerosis. Brain 135:2952–2961. https://doi.org/10.1093/brain/aws246
13. Chen C, Wu D, Fu W, Li Z (2014) Tunable Organogelator from Alkyl-Polypeptide Diblock prepared by ring-opening polymerization. Aust J Chem 67:59–65. https://doi.org/10.1071/CH13349
14. Choo LP, Jackson M, Halliday WC, Mantsch HH (1993) Infrared spectroscopic characterisation of multiple sclerosis plaques in the human central nervous system. Biochim Biophys Acta 1182:333–337. https://doi.org/10.1016/0925-4439(93)90078-f
15. Crocco MC, Moyano MFH, Annesi F, Bruno R, Pirritano D, Del Giudice F, Petrone A, Condino F, Guzzi R (2023) ATR-FTIR spectroscopy of plasma supported by multivariate analysis discriminates multiple sclerosis disease. Sci Rep 13:2565. https://doi.org/10.1038/s41598-023-29617-6
16. Demsar J, Curk T, Erjavec A, Gorup C, Hocevar T, Milutinovic M, Mozina M, Polajnar M, Toplak M, Staric A et al (2013) Orange: data mining toolbox in Python. J Mach Learn Res 14:2349–2353
17. Frischer JM, Bramow S, Dal-Bianco A, Lucchinetti CF, Rauschka H, Schmidbauer M, Laursen H, Sorensen PS, Lassmann H (2009) The relation between inflammation and neurodegeneration in multiple sclerosis brains. Brain 132:1175–1189. https://doi.org/10.1093/brain/awp070
18. Frischer JM, Weigand SD, Guo Y, Kale N, Parisi JE, Pirko I, Mandrekar J, Bramow S, Metz I, Brück W et al (2015) Clinical and pathological insights into the dynamic nature of the white matter multiple sclerosis plaque. Ann Neurol 78:710–721. https://doi.org/10.1002/ana.24497
19. Fung MFK, Senterman MK, Mikhael NZ, Lacelle S, Wong PTT (1996) Pressure-tuning fourier transform infrared spectroscopic study of carcinogenesis in human endometrium. Biospectroscopy 2:155–165. https://doi.org/10.1002/(SICI)1520-6343(1996)2:3%3c155::AID-BSPY2%3e3.0.CO;2-7
20. Gallant M, Rak M, Szeghalmi A, Del Bigio MR, Westaway D, Yang J, Julian R, Gough KM (2006) Focally elevated creatine detected in amyloid precursor protein (APP) transgenic mice and Alzheimer disease brain tissue. J Biol Chem 281:5–8. https://doi.org/10.1074/jbc.C500244200
21. Ghimire H, Hu X, Qin G, Unil Perera AG (2020) Optimizing infrared spectral discrimination to enhance disease diagnostics: monitoring the signatures of inflammatory bowel diseases with anti-TNFα therapy. Biomed Opt Express 11:4679–4694. https://doi.org/10.1364/BOE.394895
22. Haider L, Fischer MT, Frischer JM, Bauer J, Hoftberger R, Botond G, Esterbauer H, Binder CJ, Witztum JL, Lassmann H (2011) Oxidative damage in multiple sclerosis lesions. Brain 134:1914–1924. https://doi.org/10.1093/brain/awr128
23. Haile Y, Deng X, Ortiz-Sandoval C, Tahbaz N, Janowicz A, Lu J-Q, Kerr BJ, Gutowski NJ, Holley JE, Eggleton P et al (2017) Rab32 connects ER stress to mitochondrial defects in multiple sclerosis. J Neuroinflamm 14:19. https://doi.org/10.1186/s12974-016-0788-z
24. Harauz G, Ishiyama N, Hill CM, Bates IR, Libich DS, Farès C (2004) Myelin basic protein-diverse conformational states of an intrinsically unstructured protein and its roles in myelin assembly and multiple sclerosis. Micron 35:503–542. https://doi.org/10.1016/j.micron.2004.04.005
25. Heraud P, Caine S, Campanale N, Karnezis T, McNaughton D, Wood BR, Tobin MJ, Bernard CCA (2010) Early detection of the chemical changes occurring during the induction and prevention of autoimmune-mediated demyelination detected by FT-IR imaging. Neuroimage 49:1180–1189. https://doi.org/10.1016/j.neuroimage.2009.09.053
26. Jiang T, Cadenas E (2014) Astrocytic metabolic and inflammatory changes as a function of age. Aging Cell 13:1059–1067. https://doi.org/10.1111/acel.12268
27. Kawon K, Setkowicz Z, Drozdz A, Janeczko K, Chwiej J (2021) The methods of vibrational microspectroscopy reveals long-term biochemical anomalies within the region of mechanical injury within the rat brain. Spectrochim Acta A Mol Biomol Spectrosc 263:120214. https://doi.org/10.1016/j.saa.2021.120214
28. Kinder R, Ziegler C, Wessels JM (1997) Gamma-irradiation and UV-C light-induced lipid peroxidation: a Fourier transform-infrared absorption spectroscopic study. Int J Radiat Biol 71:561–571. https://doi.org/10.1080/095530097143897
29. Kołodziej M, Chrabąszcz K, Pięta E, Piergies N, Rudnicka-Czerwiec J, Bartosik-Psujek H, Paluszkiewicz C, Cholewa M, Kwiatek WM (2022) Spectral signature of multiple sclerosis. Preliminary studies of blood fraction by

ATR FTIR technique. Biochem Biophys Res Commun 593:40–45. https://doi.org/10.1016/j.bbrc.2022.01.046
30. Kucuk Baloglu F, Garip S, Heise S, Brockmann G, Severcan F (2015) FTIR imaging of structural changes in visceral and subcutaneous adiposity and brown to white adipocyte transdifferentiation. Analyst 140:2205–2214. https://doi.org/10.1039/c4an02008a
31. Kuhlmann T, Ludwin S, Prat A, Antel J, Bruck W, Lassmann H (2017) An updated histological classification system for multiple sclerosis lesions. Acta Neuropathol 133:13–24. https://doi.org/10.1007/s00401-016-1653-y
32. Lassmann H, van Horssen J (2016) Oxidative stress and its impact on neurons and glia in multiple sclerosis lesions. Biochim Biophys Acta Mol Basis Dis 1862:506–510. https://doi.org/10.1016/j.bbadis.2015.09.018
33. LeVine SM, Wetzel DL (1998) Chemical analysis of multiple sclerosis lesions by FT-IR microspectroscopy. Free Radic Biol Med 25:33–41. https://doi.org/10.1016/s0891-5849(98)00019-7
34. Lucchinetti C, Bruck W, Parisi J, Scheithauer B, Rodriguez M, Lassmann H (2000) Heterogeneity of multiple sclerosis lesions: implications for the pathogenesis of demyelination. Ann Neurol 47:707–717. https://doi.org/10.1002/1531-8249(200006)47:6%3c707::aid-ana3%3e3.0.co;2-q
35. Lucchinetti CF, Popescu BF, Bunyan RF, Moll NM, Roemer SF, Lassmann H, Brück W, Parisi JE, Scheithauer BW, Giannini C et al (2011) Inflammatory cortical demyelination in early multiple sclerosis. N Engl J Med 365:2188–2197. https://doi.org/10.1056/NEJMoa1100648
36. de Magalhães CR, Carrilho R, Schrama D, Cerqueira M, Rosa da Costa AM, Rodrigues PM (2020) Mid-infrared spectroscopic screening of metabolic alterations in stress-exposed gilthead seabream (*Sparus aurata*). Sci Rep 10:16343. https://doi.org/10.1038/s41598-020-73338-z
37. McDonald WI, Compston A, Edan G, Goodkin D, Hartung HP, Lublin FD, McFarland HF, Paty DW, Polman CH, Reingold SC et al (2001) Recommended diagnostic criteria for multiple sclerosis: guidelines from the International Panel on the diagnosis of multiple sclerosis. Ann Neurol 50:121–127. https://doi.org/10.1002/ana.1032
38. van Meer G, Voelker DR, Feigenson GW (2008) Membrane lipids: where they are and how they behave. Nat Rev Mol Cell Biol 9:112–124. https://doi.org/10.1038/nrm2330
39. Miller LM, Wang Q, Telivala TP, Smith RJ, Lanzirotti A, Miklossy J (2006) Synchrotron-based infrared and X-ray imaging shows focalized accumulation of Cu and Zn co-localized with β-amyloid deposits in Alzheimer's disease. J Struct Biol 155:30–37. https://doi.org/10.1016/j.jsb.2005.09.004
40. Nair S, Sobotka KS, Joshi P, Gressens P, Fleiss B, Thornton C, Mallard C, Hagberg H (2019) Lipopolysaccharide-induced alteration of mitochondrial morphology induces a metabolic shift in microglia modulating the inflammatory response in vitro and in vivo. Glia 67:1047–1061. https://doi.org/10.1002/glia.23587
41. Noreen R, Chien CC, Delugin M, Yao S, Pineau R, Hwu Y, Moenner M, Petibois C (2011) Detection of collagens in brain tumors based on FTIR imaging and chemometrics. Anal Bioanal Chem 401:845–852. https://doi.org/10.1007/s00216-011-4899-1
42. Obel LF, Müller MS, Walls AB, Sickmann HM, Bak LK, Waagepetersen HS, Schousboe A (2012) Brain glycogen-new perspectives on its metabolic function and regulation at the subcellular level. Front Neuroenergetics 4:3. https://doi.org/10.3389/fnene.2012.00003
43. Ohler B, Graf K, Bragg R, Lemons T, Coe R, Genain C, Israelachvili J, Husted C (2004) Role of lipid interactions in autoimmune demyelination. Biochim Biophys Acta Mol Basis Dis 1688:10–17. https://doi.org/10.1016/j.bbadis.2003.10.001
44. Patrikios P, Stadelmann C, Kutzelnigg A, Rauschka H, Schmidbauer M, Laursen H, Sorensen PS, Brück W, Lucchinetti C, Lassmann H (2006) Remyelination is extensive in a subset of multiple sclerosis patients. Brain 129:3165–3172. https://doi.org/10.1093/brain/awl217
45. Peng B, Ding X-Y, Sun C, Yang Y-N, Gao Y-J, Zhao X (2017) The chain order of binary unsaturated lipid bilayers modulated by aromatic-residue-containing peptides: an ATR-FTIR spectroscopy study. RSC Adv 7:29386–29394. https://doi.org/10.1039/C7RA01145H
46. Podbielska M, Banik NL, Kurowska E, Hogan EL (2013) Myelin recovery in multiple sclerosis: the challenge of remyelination. Brain Sci 3:1282–1324. https://doi.org/10.3390/brainsci3031282
47. Poser CM, Paty DW, Scheinberg L, McDonald WI, Davis FA, Ebers GC, Johnson KP, Sibley WA, Silberberg DH, Tourtellotte WW (1983) New diagnostic criteria for multiple sclerosis: guidelines for research protocols. Ann Neurol 13:227–231. https://doi.org/10.1002/ana.410130302
48. Rakib F, Al-Saad K, Ahmed T, Ullah E, Barreto GE, Md Ashraf G, Ali MHM (2021) Biomolecular alterations in acute traumatic brain injury (TBI) using Fourier transform infrared (FTIR) imaging spectroscopy. Spectrochim Acta Part A Mol Biomol Spectrosc 248:119189. https://doi.org/10.1016/j.saa.2020.119189
49. Reed TT (2011) Lipid peroxidation and neurodegenerative disease. Free Radical Biol Med 51:1302–1319. https://doi.org/10.1016/j.freeradbiomed.2011.06.027
50. Rohart F, Gautier B, Singh A, Lê Cao KA (2017) mixOmics: an R package for 'omics feature selection and multiple data integration. PLoS Comput Biol 13:e1005752. https://doi.org/10.1371/journal.pcbi.1005752
51. Röhr D, Boon BDC, Schuler M, Kremer K, Hoozemans JJM, Bouwman FH, El-Mashtoly SF, Nabers A, Großerueschkamp F, Rozemuller AJM et al (2020) Label-free vibrational imaging of different Aβ plaque types in Alzheimer's disease reveals sequential events in plaque development. Acta Neuropathol Commun 8:222. https://doi.org/10.1186/s40478-020-01091-5
52. Sadat A, Joye IJ (2020) Peak fitting applied to Fourier transform infrared and Raman spectroscopic analysis of proteins. Appl Sci 10:5918
53. Severcan F, Gorgulu G, Gorgulu ST, Guray T (2005) Rapid monitoring of diabetes-induced lipid peroxidation by Fourier transform infrared spectroscopy: evidence from rat liver microsomal membranes. Anal Biochem 339:36–40. https://doi.org/10.1016/j.ab.2005.01.011
54. Shaharabani R, Ram-On M, Avinery R, Aharoni R, Arnon R, Talmon Y, Beck R (2016) Structural transition in Myelin membrane as initiator of multiple sclerosis. J Am Chem Soc 138:12159–12165. https://doi.org/10.1021/jacs.6b04826
55. Simonova D, Karamancheva I (2013) Application of Fourier transform infrared spectroscopy for Tumor diagnosis. Biotechnol Biotechnol Equip 27:4200–4207. https://doi.org/10.5504/BBEQ.2013.0106
56. Toplak M, Birarda G, Read S, Sandt C, Rosendahl SM, Vaccari L, Demšar J, Borondics F (2017) Infrared orange: connecting hyperspectral data with machine learning. Synchrotron Radiat News 30:40–45. https://doi.org/10.1080/08940886.2017.1338424
57. Toplak M, Read ST, Sandt C, Borondics F (2021) Quasar: easy machine learning for biospectroscopy. Cells 10:2300
58. Trapp BD, Vignos M, Dudman J, Chang A, Fisher E, Staugaitis SM, Battapady H, Mork S, Ontaneda D, Jones SE et al (2018) Cortical neuronal densities and cerebral white matter demyelination in multiple sclerosis: a retrospective study. The Lancet Neurol 17:870–884. https://doi.org/10.1016/S1474-4422(18)30245-X
59. Wong-Ekkabut J, Xu Z, Triampo W, Tang IM, Tieleman DP, Monticelli L (2007) Effect of lipid peroxidation on the properties of lipid bilayers: a molecular dynamics study. Biophys J 93:4225–4236. https://doi.org/10.1529/biophysj.107.112565
60. Yonar D, Ocek L, Tiftikcioglu BI, Zorlu Y, Severcan F (2018) Relapsing-remitting multiple sclerosis diagnosis from cerebrospinal fluids via Fourier transform infrared spectroscopy coupled with multivariate analysis. Sci Rep 8:1025. https://doi.org/10.1038/s41598-018-19303-3
61. Zhong J, Yu W, Tang Y, Zhou X (2022) Synchrotron radiation FTIR microspectroscopy study of biomolecular alterations in vincristine-treated WRL68 cells at the single-cell level. ACS Omega 7:47274–47284. https://doi.org/10.1021/acsomega.2c06622

Publisher's Note